Journal of Dispersion Science and Technology

ISSN: (Print) (Online) Journal homepage: https://www.tandfonline.com/loi/ldis20

Facile preparation and characterization of NiO/Ni_2O_3-decorated nanoballs and mixed phase CdS nano rods (CdS&NiO/Ni_2O_3) for effective photocatalytic decomposition of Congo red under visible light irradiation

Ali İmran Vaizoğullar

To cite this article: Ali İmran Vaizoğullar (2020): Facile preparation and characterization of NiO/Ni_2O_3-decorated nanoballs and mixed phase CdS nano rods (CdS&NiO/Ni_2O_3) for effective photocatalytic decomposition of Congo red under visible light irradiation, Journal of Dispersion Science and Technology, DOI: 10.1080/01932691.2020.1814804

To link to this article: https://doi.org/10.1080/01932691.2020.1814804

JOURNAL OF DISPERSION SCIENCE AND TECHNOLOGY
https://doi.org/10.1080/01932691.2020.1814804

Facile preparation and characterization of NiO/Ni_2O_3-decorated nanoballs and mixed phase CdS nano rods ($CdS\&NiO/Ni_2O_3$) for effective photocatalytic decomposition of Congo red under visible light irradiation

Ali İmran Vaizoğullar

Vocational School of Health Care, Medical Laboratory Programme, Muğla Sıtkı Koçman University, Muğla, Turkey

ABSTRACT

This study reports the preparation of a new $CdS\&NiO/Ni_2O_3$ photocatalyst having efficient and stable photocatalytic performance. The aim was to block the photocorrosion of CdS with maintaining photocatalytic activity. The prepared CdS and NiO/Ni_2O_3 particles were in the form of nanorods and nanoballs, respectively. Diffuse reflectance spectra (DRS), X-ray diffraction (XRD), ultraviolet-visible light (UV–vis), scanning electron microscope (SEM), X-ray photoelectron spectroscopy (XPS), Raman analysis, electrochemical impedance and photoluminescence analysis were performed to evaluate structural, morphological and optical properties and their effect on photocatalytic activity. $CdS\&NiO/Ni_2O_3$ catalysts absorbed visible light and enhanced charge separation than that of CdS and NiO/Ni_2O_3. The catalytic performance of the samples was tested on Congo red. The optimal content of $CdS\&NiO/Ni_2O_3$ was observed in CN3 sample. XPS results of defective NiO with different oxygen species showed powerful photocatalytic activities. These prepared photocatalysts need to be explored further in the decomposition of various environmental pollutants.

GRAPHICAL ABSTRACT

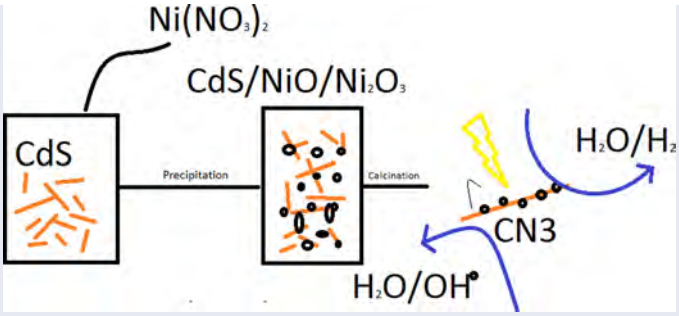

ARTICLE HISTORY
Received 28 February 2020
Accepted 16 August 2020

KEYWORDS
CdS/NiO; Congo red; defective NiO; NiO/Ni_2O_3

1. Introduction

Synthetic dyes are being used in the preparation of various industrial products such as rubber, plastic, leather, and so on. Most of the times, these dyes are not only toxic but non-degradable when go to sewage in addition to creating environmental and health problems.[1] These pollutants can lead to aesthetic pollution and perturbations in aquatic systems.[2] Consuming polluted water can cause allergy, skin irritation, liver problems, and so on. Well-known industrial pollutants are methyl orange, methylene blue, Congo red and rhodamin-B dyes.

Congo red is a carcinogenic organic pollutant that is chemically stable enough to eliminate from the environment.[3] There are physical, chemical and biological methods reported to remove Congo red and similar harmful pollutants. Membrane filtration, flocculation, ion exchange, electrochemical destruction, electro-kinetic coagulation, ozonation, adsorption, biodegradation, photocatalytic degradation and Fenton's oxidation have been also used for the same purpose.[4] From last 20 years, photocatalysis is dominating as it is cheap and feasible. Photocatalysts, which can be activated under sunlight or visible light, lead to the formation of oxidative radicals such as hydroxyls and/or superoxides. These radicals can easily degrade organic pollutants.[5]

Certain semiconductor oxides with suitable band gap energy have been studied for photodegradation of organic pollutants. Nickel oxide is an important transition metal oxide that has been used in photo-electrodes, gas sensors, lithium ion batteries, electrochemical capacitors and adsorption of water pollutants.[6] However, to apply it as a nanofibrous NiO catalyst, it must be improved to overcome strong quantum confinement effect that is lower inhibition

CONTACT Ali İmran Vaizoğullar aliimran@mu.edu.tr Vocational School of Health Care, Medical Laboratory Programme, Muğla Sıtkı Koçman University, Muğla, Turkey.

of photogenerated electron and hole species.[7] For this purpose, their incorporation over an effective catalyst support is reasonable. For example, NiO/SiO_2,[8] NiO/TiO_2,[9] NiO/ZnO[10] are based on NiO that has been synthesized and studied for catalytic applications. Incorporation of NiO onto TiO_2 can cause an inner electric field to become p-n heterojunction. The inner electric field modifies band structure at the interface that meets the impulsion of charge carriers. It also separates the electron-hole pairs by increasing the light absorption ability and extended the lifetime of charge carriers.[11] CdS is mostly used in the preparation of H_2 from water due to its strong reductive capacity.[12] CdS has some limitations such as fast recombination of charge carriers and photocorrosion that makes it difficult to be used in practical/industrial applications.[13] Therefore, a fruitful CdS-based material would be the one that separates charge carrier property and has higher utility in photocatalytic activity. For example, CdS can be used with a noble metal as s co-catalyst. However, considering the low and high cost of the noble metals, it has become imperative to develop a photocatalyst that is cheaper and can be applied on a wide scale.[14] Recently, various studies have been reported on the composite photocatalysis for example, $ZnO/CdS/Ag_2S$,[15] CdS/SiO_2,[16] ZnO/Ag_2S, [17] and so on. These composite structures possesses photochemical stability during the photocatalytic reactions. In addition, electrons exited by visible light produces electron-hole pairs after charge separation that enhances the inhibition of recombination and quantum efficiency of the composite structure.[18] Up-to-date, there are no reports on $CdS\&NiO/Ni_2O_3$ heterojunction and its photocatalysis. Therefore, it is necessary that the electronic case of a composite must be enlightened to enhance the $CdS\&NiO/Ni_2O_3$.

In the present study, $CdS\&NiO/Ni_2O_3$ composites were prepared using precipitation method. By adding different amounts of Ni_2O_3 on CdS, various $CdS\&NiO/Ni_2O_3$ composites were obtained and labeled as CN1 (1/5 mass ratio), CN2 (1/2 mass ratio) and CN3 (1/1 mass ratio), respectively. This study was aimed to explore the relationship between NiO/Ni_2O_3 and CdS in addition to the investigation of photoelectrochemical properties and photocatalytic activity. Congo Red dye was used to evaluate the photodegradation as it has azo groups where π-π^* transition occurs. It has also been widely used in textile, leather and paper industries. There are several important areas of chemical sciences where this study contributes to the photocatalytic and photoelectrochemical studies.

2. Experimental sections

2.1. Synthesis

Chemical precipitation method was used in the synthesis of CdSi, NiO and $CdS\&NiO/Ni_2O_3$. For bare CdS, 1 mL of ethylene glycol and 0.78 g NaS were dissolved in 150 mL of methanol/water mixture (2:3 v/v) and stirred for 3 h (Solution A). 0.51 g of $Cd(NO_3)_2$ was dissolved in 60 mL of water, poured into solution A and stirred for 3 h. The obtained precipitates were filtered and centrifuged for 30 min at 5000 rpm. The obtained mixture was dried in an oven at 80 °C for 3 h to obtain CdS. To prepare NiO/Ni_2O_3, 1.12 g of $Ni(NO_3)_2$ was dissolved in 100 mL of water

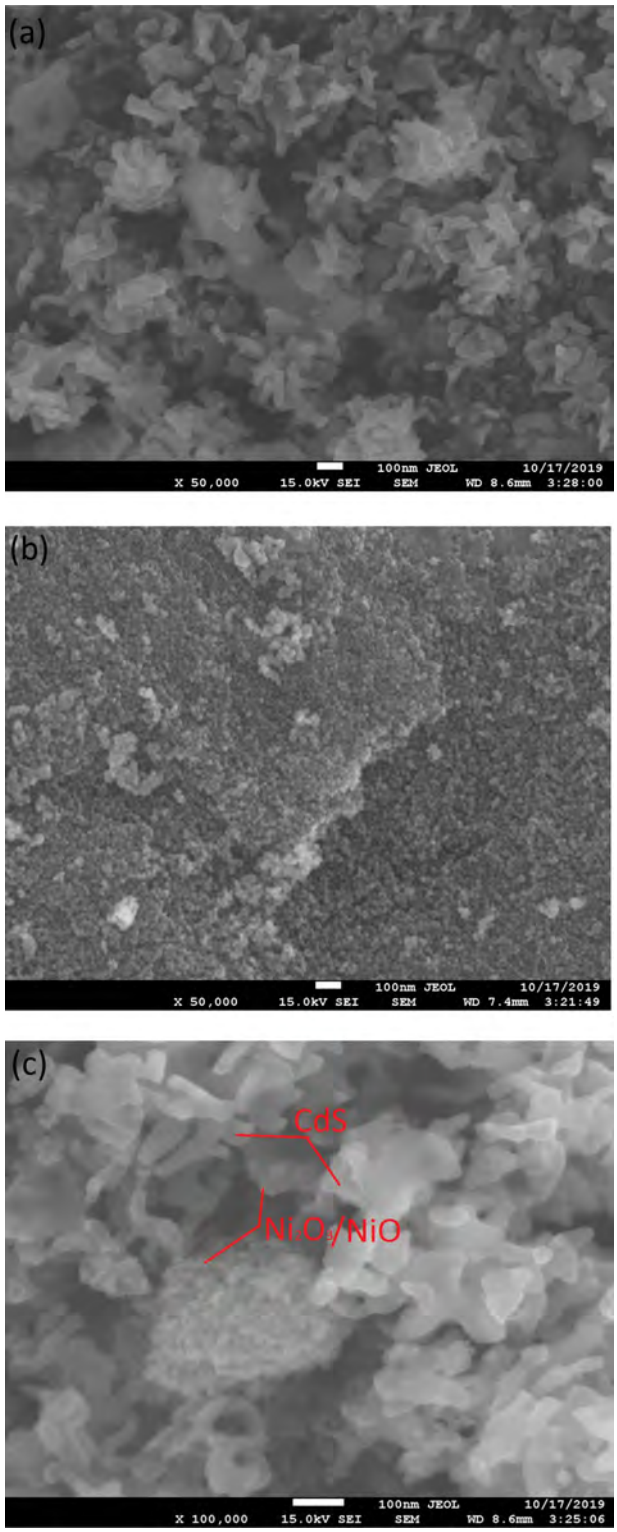

Figure 1. SEM images of CdS (a) NiO/Ni_2O_3 (b) CN3 (c) EDS results (d) Elemental mapping images of CN3 sample (e).

(Solution A). 25 mL of 0.3 mol L^{-1} NaOH solution was added to solution A. The resulted precipitates were filtered and washed with distilled water thrice. The residual sample was dried at 90 °C for 12 h followed by calcination at 350 °C. $Ni(OH)_2$ was converted to Ni_2O_3. To synthesize Ni_2O_3/CdS photocatalysts, 0.5 g of CdS was dispersed in 100 mL of water and into it, 1.125 g of $Ni(NO_3)_2$ was added slowly. $Ksp_{(NiO)}$ =

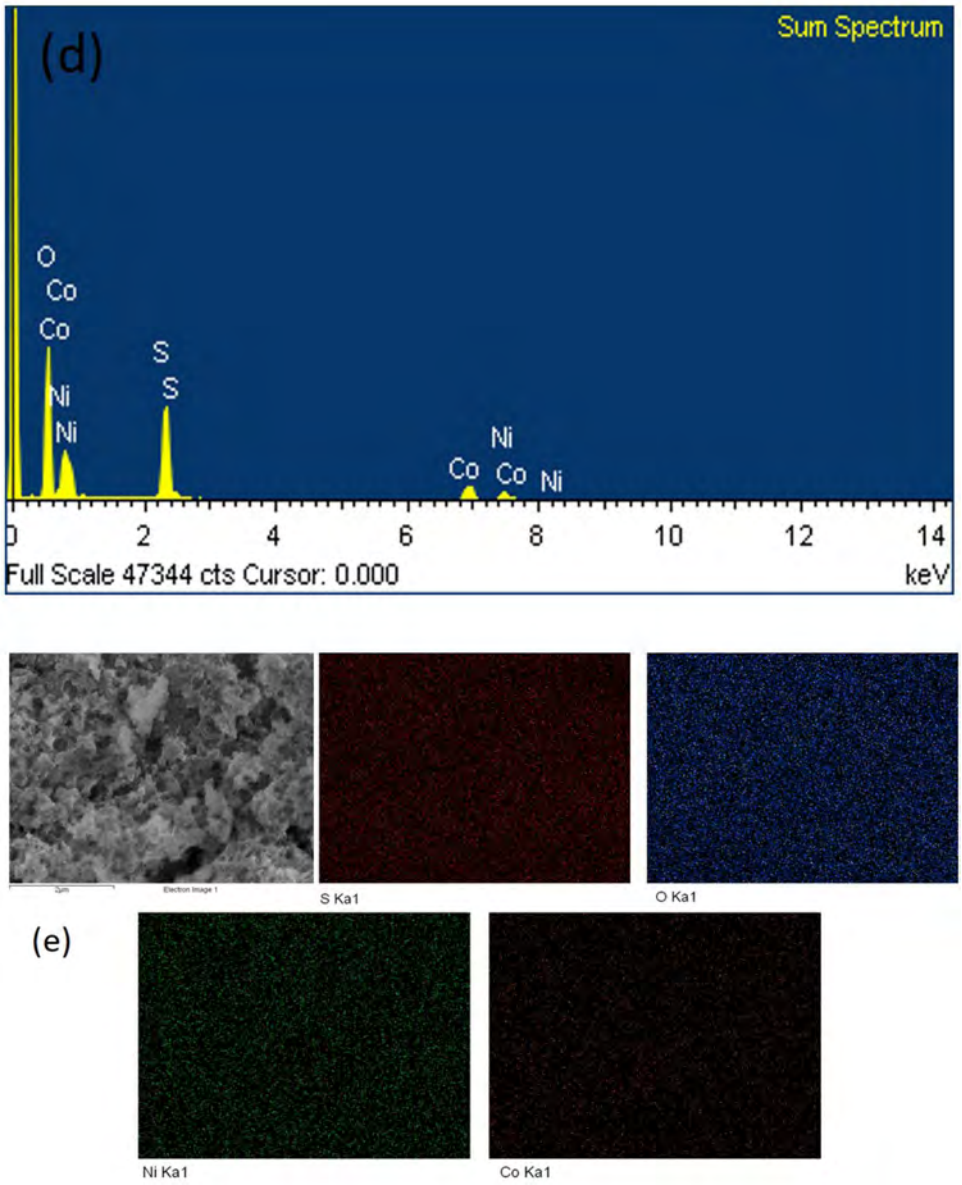

Figure 1. Continued.

1×10^{-22} and $Ksp_{(CdS)} = 8\times10^{-28}$). 0.1 mol L^{-1} of sodium hydroxide (NaOH) solution was dropped into the above mixture and stirred for 6 h. The obtained precipitates were filtered and dried at 90 °C for 120 min. The obtained $CdS/Ni(OH)_2$ solids was calcined at 300 °C for 2 h. This reaction is represented as follows:

$$CdS/Ni(OH)_2 \xrightarrow{\text{Calcined at } 300\ C^{o}} CdS\delta NiO/Ni_2O_3$$

Synthesized composite materials with various amounts of Ni_2O_3 were identified as CN1, CN2 and CN3, respectively.

2.2. Characterization

Morphology of the synthesized particles were investigated using SEM (JEOL JSM-7600F). The crystalline structures were investigated by x-ray diffraction (XRD: Rigaku D/MAX 350) using copper K radiation (k = 0.154 nm). X-ray photoelectron spectroscopic (XPS) measurement was performed using a PHI 5000 Versa Probe. The optical properties of the solid samples (UV–vis DRS) were performed using a Lambda 35 UV–vis spectrophotometer. The photoluminescence (PL) spectra of photocatalysts were measured using spectrofluorometric (Spex 500 M, USA) PL emission by 532 nm lasers. The electrochemical impedance spectra (EIS) were analyzed by an impedance analyzer (Gamry Potantiostate/Galvanostat/ZRA Reference 3000) using a standard three-electrode system with the samples as the working electrodes, a saturated calomel electrode (SCE) as the reference electrode, and a Pt wire as the counter electrode. Frequency operating range was 1 kHz–107 Hz. Raman analyses were performed at room temperature using Raman spectrophotometer (Bruker IFS 66/S, FRA 106/S, HYPERION 1000, RAMANSCOPE II).

2.3. Photocatalysis

Photocatalysis was performed under sunlight to decompose Congo red. In this experiment, 0.25 g of photocatalyst was added

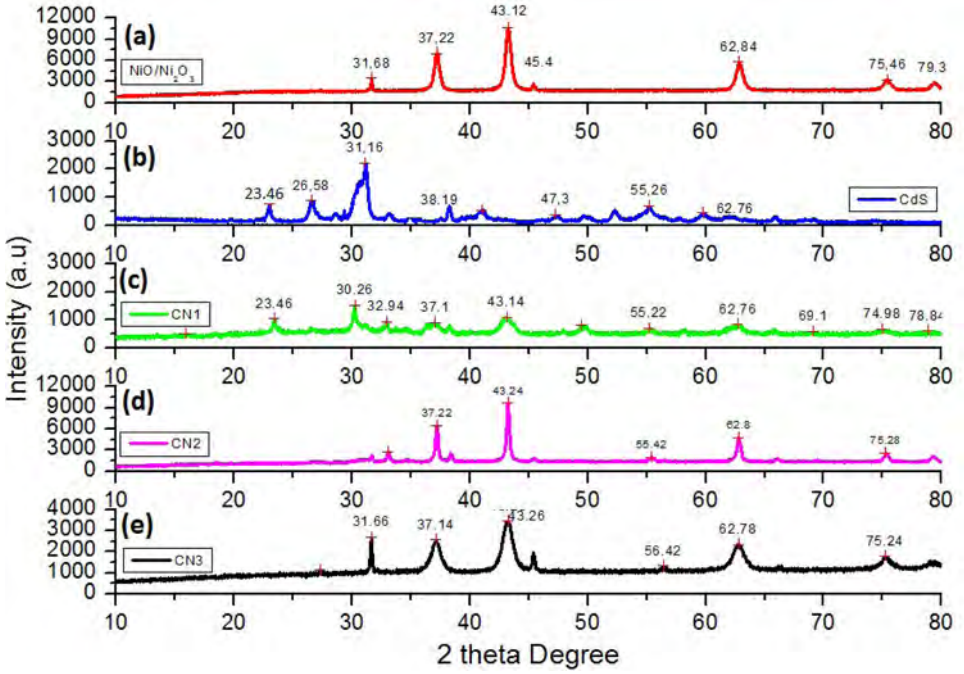

Figure 2. XRD pattern of bare and composite photocatalysts.

to 100 mL of Congo red dye solution (10 ppm). The solution was stirred for 30 min to achieve adsorption/desorption equilibrium. After irradiation, 3 mL of aliquot was taken to measure absorbance in a UV–Vis spectrophotometer. Congo red shows λ_{max} at 495 nm. Each measurement for residual Congo red dye and absorbance was carried out after every 30 min. Degradation efficiency was calculated using the following formula:

$$\%\text{Degradation} = \frac{C_0 - C}{C_0} \times 100 = \frac{A_0 - A_t}{A_t} \times 100$$

where A_0 and A_t are the initial and final absorbencies of Congo red at 495 nm. According to Beer–Lambert law, the initial and final absorbencies are directly proportional to the initial and final concentrations, respectively.

3. Results and discussion

3.1. SEM analysis

Figure 1 shows the results of SEM analysis of the synthesized particles. CdS particles have an irregular rod structure (Figure 1a) with approximately 30 nm wide and 100 nm long. On the other hand, Ni_2O_3 particles were microball-shaped with 510 nm diameter (Figure 1b). Furthermore, these particles were regularly decorated with no gaps between them. SEM analysis of composite particles clearly shows that both components have formed the composite structure with their characteristic features (Figure 1c). However, micro-ball Ni_2O_3 particles were not regularly decorated within the composite structure. Furthermore, one part of Ni_2O_3 is decoratively dispersed on the CdS probably due to their applomeration as the temperature increases. In addition, due to the small dimensions and rough surfaces, the resulting CdS&NiO/Ni_2O_3 composites could have a large specific surface area that is useful for adsorption and photocatalysis.[19]

The elemental composition of CN3 was investigated by EDS. The target elements that is, Cd, Ni, O and S are clearly seen in EDS spectra (Figure 1d). Although the changes in the morphological structures of CdS and Ni_2O_3 affects the catalytic performance, this study did not cover the effect on photocatalytic performance as the morphology did not changed. SEM images also present the formation of binary hybrid composite (Figure 1e). The elemental analysis shows the homogenous distribution of Cd, O, Ni and S atoms in CN3. Also, the SEM elemental mapping analysis shows less color intensity of Cd than that of Ni. It means that NiO is more disperse on CdS. The same is true for oxygen and sulfur atoms.

3.2. XRD analysis

One can easily get the structural properties of various materials using XRD analysis. Figure 2 presents the XRD results of all photocatalysts. From Figure 2a (NiO/Ni_2O_3), the diffraction peak at 31.67°, 45.41° and 75.29° degree attributes to (202), (111) and (311) plane of Ni_2O_3. Also, 37.67°, 43.22°, 62.80° and 79.36° corresponds to (111), (200), (220) and (222) plane, respectively. These results confirm the cubic structure of Ni_2O_3 and hexagonal structure of NiO. For CdS, the diffraction peaks at 23.46°, 26.58°, 38.19°, 47.31°, 55.26°, 62.76°, 69.11° and 74.98° corresponds to (100), (002), (101), (102), (202), (104), (211) and (105) planes of the wurtzite hexagonal structure (JCPDS 41–1049), respectively.[20] One peak at 31.16° corresponds to (220) plane of cubic CdS confirming the mixed phase of cubic and hexagonal CdS.

Figure 2c–e shows XRD diffraction peaks of composite samples where the characteristic diffraction peaks of both NiO/Ni_2O_3 and CdS are clearly seen. However, some diffraction peaks such as ~23°, ~38°, ~47°, ~69° were not

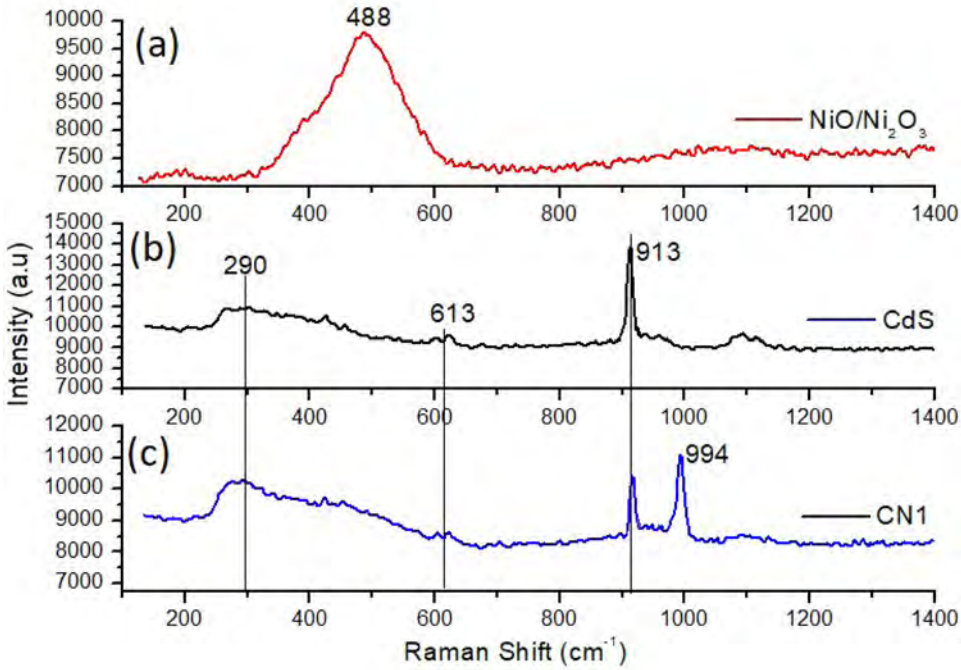

Figure 3. Raman spectra of NiO/Ni_2O_3 (a), CdS (b) and CN3 composites (c).

observed in CN2 and CN3 composites probably due to the dispersion of NiO/Ni_2O_3 on CdS. Considering the XRD peaks of composites, even though all composites were calcined at the same temperature, the CN2 sample has sharper peaks. This indicates that not only CN2 sample is better crystallized, but also the optimum amount of NiO/Ni_2O_3 affects the crystal structure of the composite. The absence of characteristic peak of the cubic CdS at ~31.16° supports this explanation. Considering that the figure is examined, the characteristic 2θ degree of Ni_2O_3 at 31.68 did not change in the composite samples, while the characteristic main peak of the NiO which was present at 37.18° have shifting toward lower angles. On the other hand, the characteristic CdS peaks in the composite samples were shifted to slightly higher angles. As well known, XRD peak due to strain and planer stress or changing in the composite stoichiometry can increase of decrease, which corresponds the compressive and tensile stress.[21] According to obtained data, we can infer that both stresses are available in the composite sample. This finding, while preliminary, also suggests that an effective photocatalytic performance should be obtained with composite materials.

The crystalline size of catalysts was calculated with Scherrer equation referenced using the most intense peak using the following equation:

$$d = \frac{0.9 \times \lambda}{FWHM(Radian) \times Cos\theta} \quad [1]$$

The crystalline size of the composites decreased with loading NiO/Ni_2O_3 on CdS (Table 1)These findings must help us to understand that decreasing particle size made it difficult to see the characteristic peaks of CdS in XRD diffraction pattern.[22]

Table 1. d value of photocatalysts sample as Angstrom unit.

Sample	d(Å)	NiO/Ni_2O_3	CdS
NiO/Ni_2O_3	2.09	–	–
CdS	2.91		
CN1		2.95	3.79
CN2		2.41	1.65
CN3		2.09	1.62

3.3 Raman spectra

Figure 3 shows the Raman analysis of all catalysts. The confinement of phonon, strain, defect and broadening significantly affects the Raman spectra of nanostructure. In Figure 3a, the band seen at 488 cm^{-1} is probably the Ni^{3+} and overlapping 1LO phonon peak of Ni^{2+}.[23] In Figure 3b, CdS shows two Raman active peaks. The peaks appeared at 290 and 613 cm^{-1} are attributed to the first and second order longitudinal (LO) modes. The absence of a change in the 1LO and 2LO modes also indicates that there is no change in the shape of CdS particles (Figure 3c). In this case, multi-phonon scattering occurs and weak Raman bands at ~340 can be observed.[24] As seen from Figure 3b, 3LO mode of CdS is observed at 913 cm^{-1}. Furthermore, 1 LO and 2 LO modes of CdS are much fainter than 3 LO mode of CdS. A possible explanation for this might be that, phonon confinement occurs in the transverse directions while elementary excitation has occurred in the longitudinal direction. In this case, enhanced exciton-LO phonon coupling in the CdS sample has been observed significantly.[25] After composition of CdS with NiO/Ni_2O_3, Raman scattering presents a magnon peak (2 M) behind 1LO and 2LO phonon of CdS. 2 M peak at 994 cm^{-1} shows a 3-dimensional, cubic and antiferromagnetic material that is supported by XRD results. 2 M peak also exhibits the anti-ferromagnetic property of the material, which is the same as ferro-magnetism that

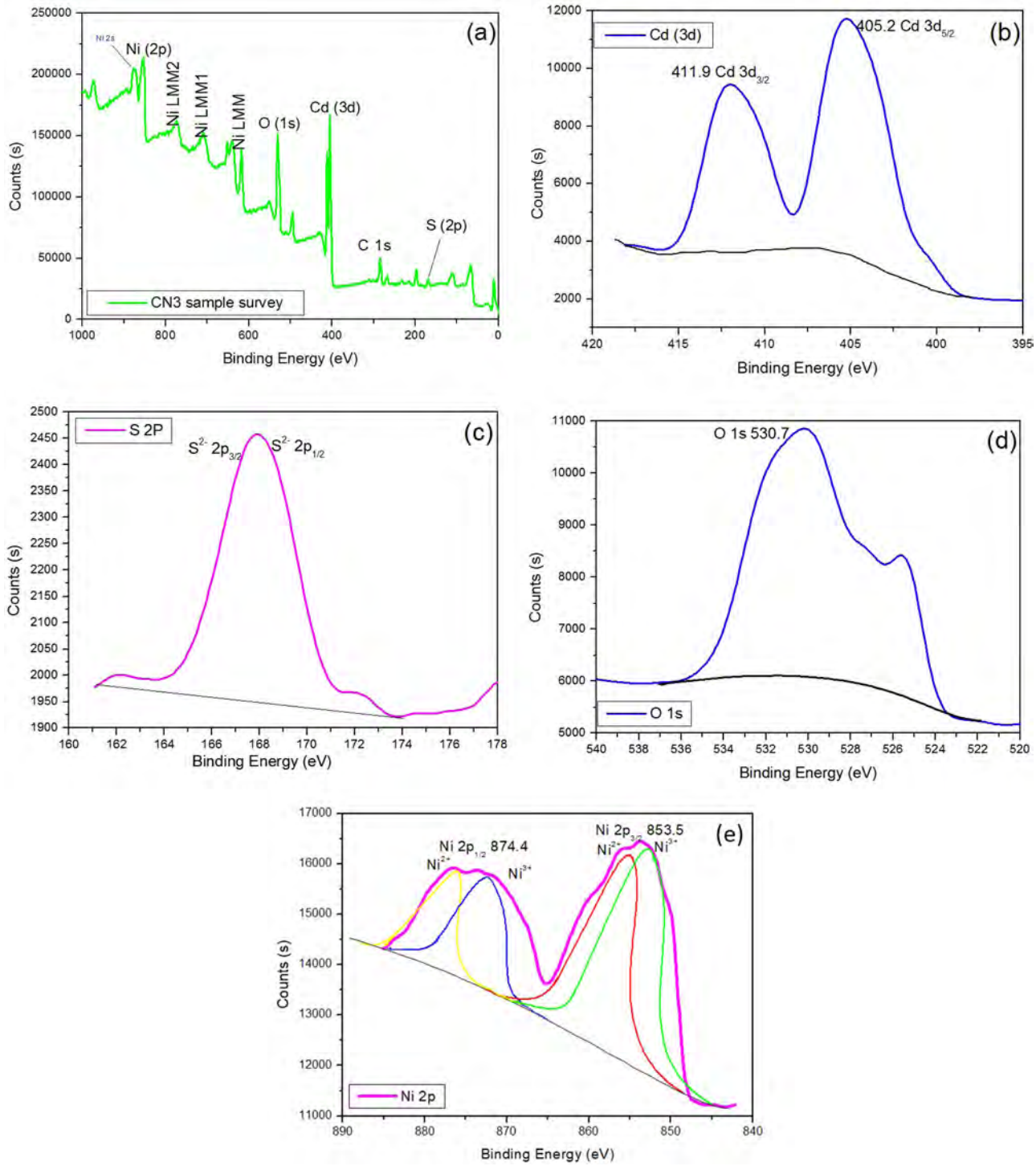

Figure 4. XPS analysis of CN3 photocatalyst: (a) Survey spectrum; (b) Cd 3d; (c) S 2p; (d) O 1 s; (e) Ni 2p.

explains the attraction of materials toward the external magnet.[26] The band at 994 cm^{-1} is sharper while the other 1LO and 2 LO peaks are broader. These results confirmed the production of CdS&NiO/Ni_2O_3 composites, partial changes in the crystalline structure and reduction of defect. Previous studies have presented that 1 LO, 2LO and 3LO vibrational mode of CdS occurs at 300, 600 and 900 cm^{-1}, respectively. The LO phonons observed in the Raman bands shows the fracturing of selection rules because of the electronic resonance where electrostatic forces dominates over the anisotropy.[27] Furthermore, due to the confinement effect, 1LO and 2LO bands have broadening and downward shift confirming the tensile or compressive strain that causes red or blue shift in the Raman spectra. In the present study, all LO bands in bare CdS and CN1 composite shows lower frequency (Figure 3c). This observation may support the hypothesis that there is a higher phonon confinement and strong electronic coupling at the interface or large number of defect sites (compressive stress) in the composites.[28] Surprisingly, the characteristic Ni^{2+}/Ni^{3+} bands observed in Figure 3a were not observed in the Raman spectra

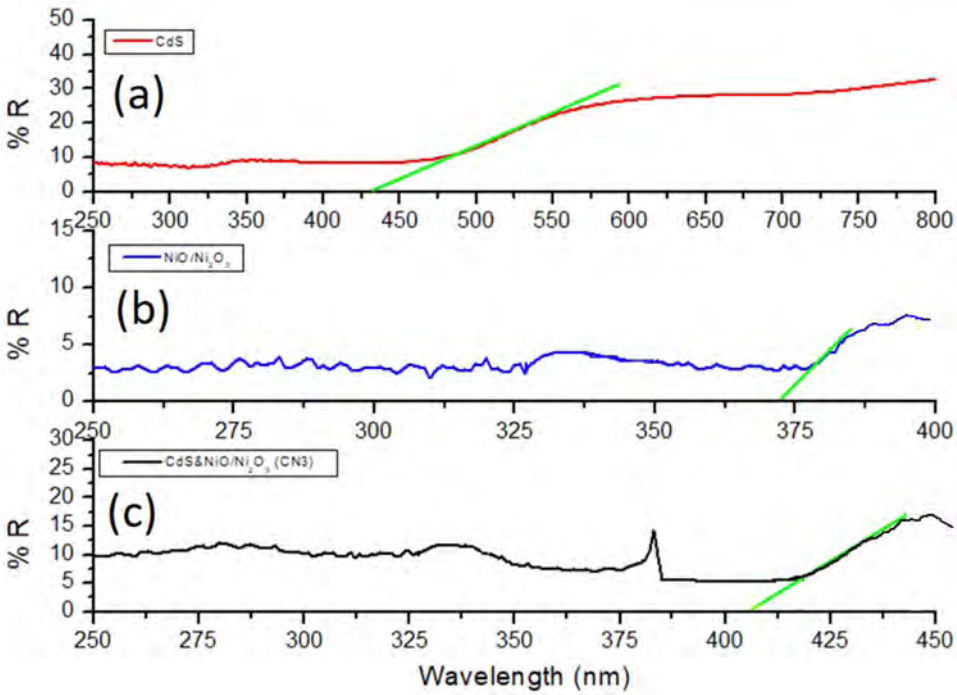

Figure 5. UV-DRS spectra of the synthesized photocatalysts.

of CN3 composite. Similarly, the 2 M magnon bands were not observed in Figure 3a.

3.4. XPS analysis

To explain the chemical states of the elements in CdS&NiO/Ni_2O_3 (CN3), XPS analysis was performed. Figure 4a shows the XPS results of CN3 between 200 and 1000 eV binding energy. Target elements that is, Cd, S, Ni and O were observed in CN3. Figure 4b shows Cd 3d peaks at 405.2 and 411.9 eV binding energy that represents the Cd $3d_{5/2}$ and Cd $3d_{3/2}$, respectively. A spin orbit coupling of 6.7 eV significantly confirms the presence of Cd in the photocatalysts in the form of Cd^{2+}.[29] Figure 4c displays S 2p binding energy at 164-169 eV corresponds to $2p_{3/2}$ and $2p_{1/2}$. This indicates S^{2-} form bridging S atoms.[30] Figure 4c shows O 1 s binding energy at 530.7 eV in the CN3 photocatalyst. It is clearly attributed to O^{2-} oxidation state in the NiO/Ni_2O_3. The binding energy at 525 eV in the O 1 s of XPS results shows the formation of new oxygen species due to a change in the oxygen coordination.

Figure 4edisplays Ni 2p spectra where the peaks at 853.5 and 874.4 eV corresponds to Ni $2p_{3/2}$ and Ni$2p_{1/2}$, respectively. In addition, when the XPS spectra of Ni 2p showed both Ni^{2+} and Ni^{3+} species. These results indicate a defective NiO in the CN3 sample that is also supported by O 1 s XPS spectra.[31]

3.5. UV–Vis analysis

To explain the optical properties of bare and composites (CN3), UV-DRS studies were performed between 200 and 800 nm (Figure 5). Bare CdS and NiO/Ni_2O_3 samples showed broad and sharper absorption peaks, respectively, in the UV–visible spectra (Figure 5a and b). For composite CN3, broad absorption peak can be seen in the visible region (Figure 5c). The band gap of each catalyst was estimated with the following formula:

$$E_g = \frac{1240}{\lambda} \quad [2]$$

The absorption peaks of CdS, NiO/Ni_2O_3 and CN3 are 426, 372 and 405 nm that corresponds to the band gap of 2.91, 3.34 and 3.06 eV, respectively. After loading CdS on NiO/Ni_2O_3, the absorption peak shifted to visible area in case of CN3 composite that confirms the spread and incorporation of CdS into the crystalline structure of CN3. Thus, composite samples are expected to increase the photocatalytic degradation under visible light. The ECB and EVB values can be calculated from the following equations:

$$E_{CB} = \delta - E_E - 0.5 \times E_g \text{ and } E_{VB} = E_{CB} + E_g \quad [3]$$

where δ is the electronegativity of CdS (5.18 eV)[32] and E_E is the energy of free electron on the hydrogen scale (NHE, 4.5 eV). E_{CB}, E_{VB} and E_g are conduction band, valence band and band gap values, respectively. The E_{CB}, and E_{VB} values were calculated as −0.775 and 2.135 eV for CdS while −0.405 and 2.925 eV for NiO/Ni_2O_3, respectively. When CdS&NiO/Ni_2O_3 sample is irradiated by visible light, the E_{VB} electrons of CdS excites to E_{CB} level. To form a new Fermi level equilibrium, electrons flows from CdS to NiO/Ni_2O_3. In this case, the electric field forms by electrostatic induction can quickly drive the electron/hole pairs by absorbing the suitable photons of CdS&NiO/Ni_2O_3.[33]

The redox potential of superoxide $O2/O_2^{\bullet -}$ is aprox. −is aprox Transferring of electrons from NiO can produce superoxide ($O_2^{\bullet -}$) radicals with O2 as it is more negative than the potential of $O2/O2^{\bullet -}$. However, E_{VB} potential of CdS is more negative than the standard redox potential of $OH^-/OH^{\bullet}$ (2.40 eV). The transferred holes (h^+) from E_{VB}

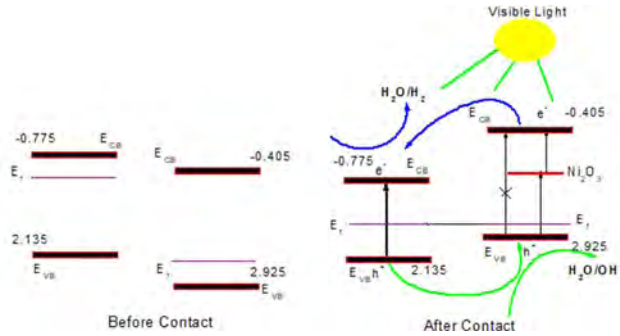

Scheme 1. The proposed mechanism of photocatalytic degradation.

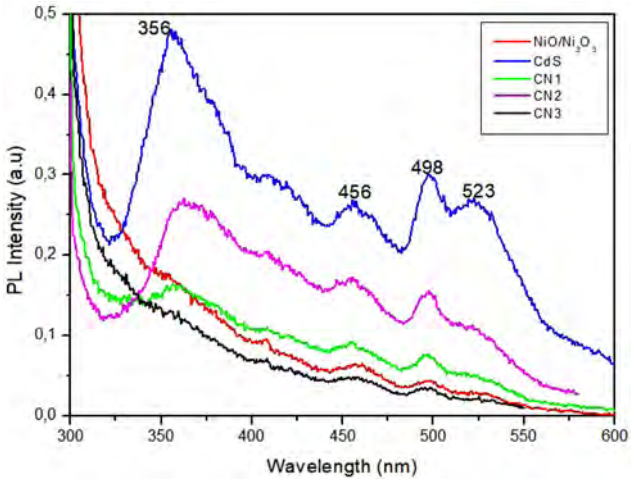

Figure 6. PL spectra of the synthesized photocatalysts.

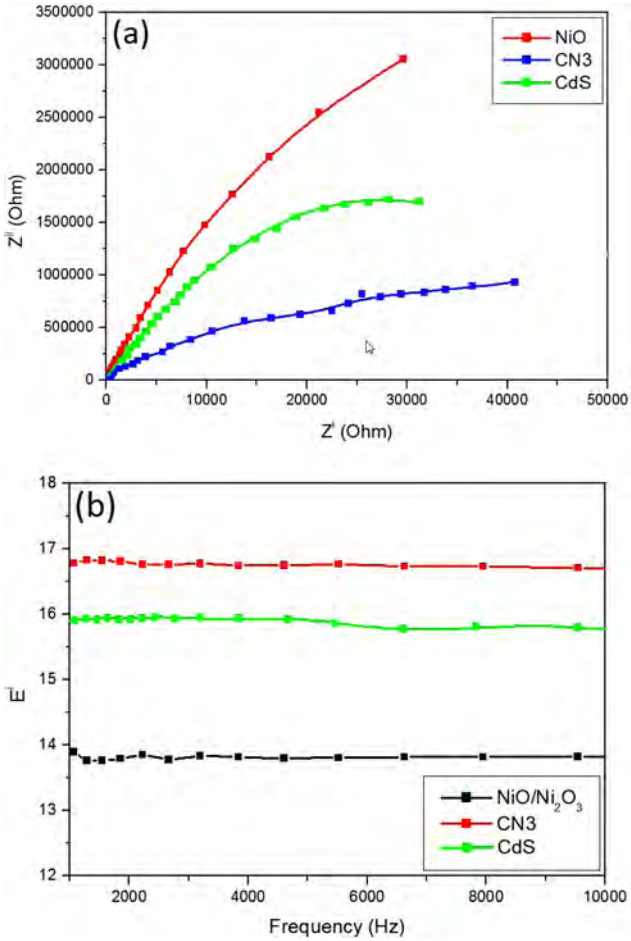

Figure 7. Electrochemical analysis of CdS, NiO/Ni_2O_3 and CN3 sample: (a Nyquist plots; b) dielectric constants.

level of CdS could reveal $OH^{\bullet}$ radicals. It is possible that, the lower photocorrosion occurs on CdS in CdS&NiO/Ni_2O_3 composite. It further confirms the transfer of photogenerated holes to E_{VB} level of NiO/Ni_2O_3.

The possible degradation mechanism was also investigated. As well known, NiO is p-type while CdS is the n-type semiconductor. The possible degradation mechanism is presented in Scheme 1.

3.6. Photoluminescence (PL)

To explain the photoexcited charge transfer process in the NiO/Ni_2O_3&CdS composites, PL analysis of bare and composite samples were performed. PL spectra (Figure 6) of NiO/Ni_2O_3 (Red line) show three emission peaks at 458, 497 and 527 nm, respectively. The peak at 458 and 491 attributed to the presence of Ni interstitial sites as well as the surface defects.[34] The red emission peak at 527 nm reveals the oxidation of Ni^{2+} to Ni^{3+}.[35] In case of CdS, spectra (Blue line) presented four emission broad peaks at 356, 456, 498 and 523 nm. The visible emissions of CdS can be related to different intrinsic defects such as sulfide and cadmium vacancies, and interstitials. The peak at around 523 nm has originated from recombination of donor-acceptor pairs.[36] The peaks around 356 and 456 nm are due to high energy photons that can be related to the higher level of emission from quantum confinement.

All synthesized photocatalysts showed similar spectra where three peaks appeared at near 456, 487 and 523 nm are the peaks corresponding to purple, blue and green light in the visible region, respectively. The band at 523 nm can be attributed to the near-band emission that is derived from the recombination of electrons. The other bands at 456 and 487 nm usually attributed to excitons connected ionized donors and/or the shallow trapped electron-hole pairs. This is also indicating the intrinsic properties and defect level that is particularly from the grain defects or different morphological structures of CdS. These findings are consistent with the study published by Cai et al. [37] As previously reported, lower PL intensity means the inhibition of recombination of charge carriers. The PL intensity of CN3 is much lower than that of CN1 and CN3 indicating the formation of p-n heterojunction and higher inhibition of electron-hole pairs at the surface of the catalyst.[38] Surprisingly, the PL intensity of CN2 catalyst was higher than that of CN1 (Figure 6). Generally, lower PL intensity shows a lower recombination, however, there are exceptions. Sometimes, as the number of oxygen surface defects and oxygen vacancies increases on the surface of the catalyst, high photocatalytic activity can be observed with an increase in the PL intensity. As there is a possibility, CN2 catalyst showed higher PL intensity.

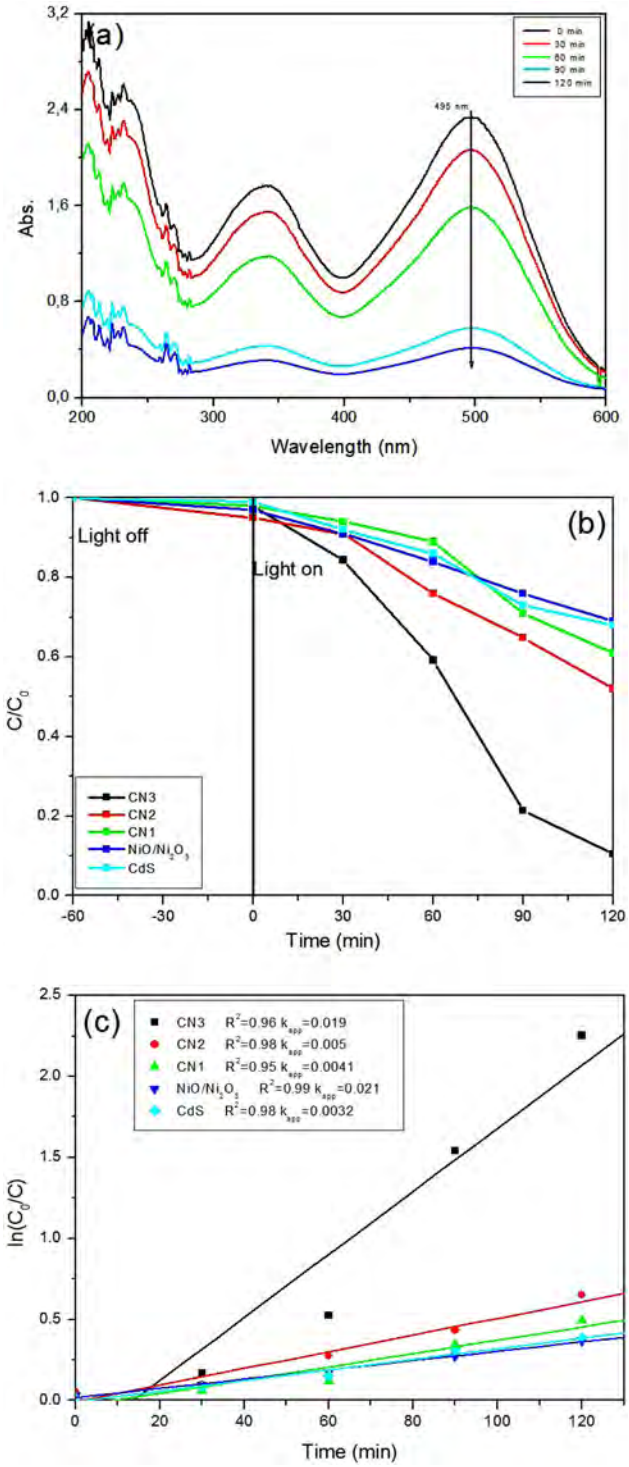

Figure 8. UV–Vis spectra of Congo red for 120 min with (a) CN3 sample; (b) Degradation yield of catalysts; (c) Pseudo first-order kinetic rates.

3.7. Electrochemical impedance and dielectric properties

EIS was investigated under visible light to understand the charge separation behavior. As, known, the real and imaginary Z values of the electrochemical impedance spectrum are obtained depending on the capacitance and resistance values of the components in the electrochemical cell. In general, a Nyquist plot presents more semicircular arcs with diameter along the Z_{real} axis. The smaller arc radius specifies the faster rate of interface charge carrier transfer. CN3 composite showed the least semicircle arc (Figure 7a) as compared to the bare CdS and NiO/Ni_2O_3 samples. This confirms an improved transfer behavior of CN3 for the photoexcited carriers.[39] Comprehensively, small arc radius displays lower electron transfer resistance at surface.

Figure 7b shows the dielectric constants with frequency at room temperature. The dielectric constant linearly decreased with frequency at a constant working temperature. Dielectric constant of CN3 was higher than that of CdS and NiO/Ni_2O_3; probably due to the defect level, that magnifies polar centers in the CN3. This also supports the electronic interactions between the electro-active metal centers that can reinforce electron transport in the composites and subsequently elevate electro-catalytic activity and electronic properties.[40,41]

3.8. Photocatalytic degradation of Congo red

Figure 8a shows the degradation spectra of Congo red using the CN3 sample at λ_{max} 495 nm. Effective degradation has been achieved within 120 min. The photocatalytic degradation activity of Congo red solution under visible light irradiation using the NiO/Ni_2O_3, CdS and composite samples (CN1, CN2, CN3) has been plotted as C_t/C_0 in Figure 8b and c, respectively. There are three possible degradation ways for organic dyes that is, photosensitization, photolysis, and photocatalysis.[42] The decomposition of Congo red in the presence of NiO/Ni_2O_3 and CdS within 120 min under visible light irradiation is very tenuous (Figure 8b) that is 28 and 31%, respectively. On the other hand, CN3, CN2 and CN1 showed 82, 60 and 44% photodegradation, respectively. These results are higher than some of the reported oxide-based metals. Results showed that CdS&NiO/Ni_2O_3 composites have higher degradation performance than that of bare CdS and NiO/Ni_2O_3. Moreover, the photocatalytic degradation increased with increasing the molar content of CdS. We can infer that there is an optimal content of the components in the catalyst structure.

The pseudo first-order kinetic rate is plotted as a function of time (Figure 8c). The kinetic rate constant (k) was calculated from the slope of $-\ln(C/C_0)$ versus time. The calculated k values were 0.019 min^{-1} for CN3 sample presenting the highest photocatalytic activity compared to other samples. This is also 6 and 9 times higher than that of NiO/Ni_2O_3 and CdS, respectively. This higher degradation performance can be explained as follows; (i) An effective inhibition of photogenerated electron/hole pairs (ii) Optimal content of CdS in the composite structure with light absorption ability (iii) effective active sites of cadmium interstitials or oxygen vacancies.

As well known, the Fermi levels for p and n semiconductor heterojunctions are close to the VB and CB band levels, respectively. It also supports the formation of an internal electrical field. After contact, the energy bands of NiO shifts upward while the energy band of CdS shifts downward. This fact indicates the separating of charge carries thermodynamically. Scheme 1 shows a proposed

degradation mechanism of CN3. A heterojunction was obtained between CdS and NiO/Ni_2O_3. A new Fermi level was formed due to the flow of electrons from CdS to NiO/Ni_2O_3. When visible light is irradiated on CN3, the electric field is formed by electrostatic induction in the electron-hole diffusion near the p-n interface reveals until the Fermi level equilibrium is achieved; also called as internal electric field. After contact, the excited electrons of CdS, which are more electronegative can produce H_2 or superoxide radicals $(O_2^{\cdot-})$ while VB electrons of NiO/Ni_2O_3 can be excited to CB level by two Ni species (Ni^{2+}, Ni^{3+}). In this case, the electrons in the CB level of NiO/Ni_2O_3 can be transferred to CB level of CdS. The photoinduced holes are transferred from VB level of NiO/Ni_2O_3 to block the photocorrosion of CdS whereas hydroxyl radicals are obtained due to more electropositive band level under the influence of internal electric field. These mechanisms result the spatial separation of charge carriers and significantly extend their lifetime. In the light of these statements, more active catalytic performance of CN3 can be attributed to the following points. (i) Extended light absorption caused the yield of charge collection. In addition, more charge carriers can be produced upon visible light irradiation. (ii) An excellent band alignment in the CdS&NiO/Ni_2O_3 (CN3) photocatalyst increased the inhibition and recombination of electron hole pairs. From another perspective, the excited electrons can be captured by Ni^{3+} due to more electronegative redox potential and irreversible reaction $(Ni^{3+} + e^- \rightarrow Ni^{2+} = -2.94\ V)$.

4. Conclusion

It this study, the CdS&NiO/Ni_2O_3 photocatalyst was successfully fabricated via facile precipitation and calcination methods. CdS&NiO/Ni_2O_3 composites were characterized and used for photodecomposition of Congo red under visible light irradiation. The structural properties and p-n heterojunction phenomenon plays a major role in photocatalytic degradation. The composite CdS&NiO/Ni_2O_3 sample showed better photocatalytic activity than that of bare CdS and NiO/Ni_2O_3. Also, CN3 sample presented more catalytic performance than that of other CN1 and CN2 that was attributed to the optimal content of NiO/Ni_2O_3 onto CdS and excellent band alignment among them. This work shed a beneficial light on the future studies based on nickel and cadmium photocatalysts.

.

Funding

This work was supported by Muğla Sıtkı Koçman University Coordination of Scientific Research Project Unit with 19/088/01/1/1.

ORCID

Ali İmran Vaizoğullar http://orcid.org/0000-0003-4369-405X

References

[1] Song, Z.; Chen, L.; Hu, J.; Richards, R. NiO(111) Nano Sheets as Efficient and Recyclable Adsorbents for Dye Pollutant Removal from Wastewater. *Nanotechnology* **2009**, *20*, 275707. DOI: 10.1088/0957-4484/20/27/275707.

[2] Sauer, T.; Neto, G. C.; Jose, H. J.; Moreira, R. F. P. M. Kinetics of Photocatalytic Degradation of Reactive Dyes in a TiO_2 Slurry Reactor. *J. Photochem. Photobiology A: Chem.* **2002**, *149*, 147–154. DOI: 10.1016/S1010-6030(02)00015-1.

[3] Doke, K. M.; Yusufi, M.; Joseph, R. D.; Khan, E. M. Comparative Adsorption of Crystal Violet and Congo Red onto $ZnCl_2$ Activated Carbon. J Disper Sci Technol. 2016, 37, 1671–1681.

[4] Shaban, M.; Abukhadra, M. R.; Hamd, A.; Amin, R. R.; Khalek, A. A. Photocatalytic Removal of Congo Red Dye Using MCM-48/Ni_2O_3 Composite Synthesized Based on Silica Gel Extracted from Rice Husk Ash; Fabrication and Application. *J. Environ. Manage.* **2017**, *204*, 189–199. DOI: 10.1016/j.jenvman.2017.08.048.

[5] Sun, D.; Zhang, Z.; Wang, M.; Wu, Y. Adsorption of Reactive Dyes on Activated Carbon Developed from Enteromorpha Prolifera. *AJAC.* **2013**, *04*, 17–26. DOI: 10.4236/ajac.2013.47A003.

[6] Sun, W.; Chen, L.; Meng, S.; Wang, Y.; Li, H.; Han, Y.; Wei, N. Synthesis of NiO Nanospheres with Ultrasonic Method for Supercapacitors. *Mat. Sci. Semicon. Proc.* **2014**, *17*, 129–133. DOI: 10.1016/j.mssp.2013.09.002.

[7] Torki, F.; Faghihian, H. Visible Light Degradation of Naproxen by Enhanced Photocatalytic Activity of NiO and NiS, Scavenger Study and Focus on Catalyst Support and Magnetization. *Photochem. Photobiol.* **2018**, *94*, 491–502. DOI: 10.1111/php.12906.

[8] Jeong, M. G.; Park, E. J.; Jeong, B.; Kim, D. H.; Kim, Y. D. Toluene Combustion over NiO Nanoparticles on Mesoporous SiO_2 Prepared by Atomic Layer Deposition. *Chem. Eng. J.* **2014**, *237*, 62–69. DOI: 10.1016/j.cej.2013.09.100.

[9] Zhu, L.-W.; Li, H.-X.; Ren, Z.-G.; Wang, H.-F.; Yao, W.; Lang, J.-P. Engineering Growth of TiO_2 Nanofibers on NiO–Ni Foam with Cleaning and Separation Functions. *RSC Adv.* **2013**, *3*, 15421–15426. DOI: 10.1039/c3ra40634b.

[10] An, X.; Zhang, Y. Fabrication of NiO Quantum Dot-Modified ZnO Nanorod Arrays for Efficient Photoelectrochemical Water Splitting. *Appl. Phys. A* **2017**, *123*, 647. DOI: 10.1007/s00339-017-1237-2.

[11] Sharma, A.; Lee, B. K. Integrated Ternary Nanocomposite of TiO_2/NiO/Reduced Graphene Oxide as a Visible Light Photocatalyst for Efficient Degradation of o-Chlorophenol. *J. Environ. Manage.* **2016**, *181*, 563–573. DOI: 10.1016/j.jenvman.2016.07.016.

[12] Yin, X. L.; Li, L. L.; Jiang, W. J.; Zhang, Y.; Zhang, X.; Wan, L. J.; Hu, J. S. MoS_2/CdS Nanosheets-on-Nanorod Heterostructure for Highly Efficient Photocatalytic H_2 Generation under Visible Light Irradiation. *ACS Appl. Mater. Interfaces.* **2016**, *8*, 15258–15266. DOI: 10.1021/acsami.6b02687.

[13] Wu, K.; Du, Y.; Tang, H.; Chen, Z.; Lian, T. Efficient Extraction of Trapped Holes from Colloidal CdS Nanorods. *J. Am. Chem. Soc.* **2015**, *137*, 10224–10230. DOI: 10.1021/jacs.5b04564.

[14] Chen, W.; Wang, Y.; Liu, M.; Gao, L.; Mao, L.; Fan, Z.; Shangguan, W. In Situ Photodeposition of Cobalt on CdS Nanorod for Promoting Photocatalytic Hydrogen Production under Visible Light Irradiation. *Appl. Surf. Sci.* **2018**, *444*, 485–490. DOI: 10.1016/j.apsusc.2018.03.068.

[15] Chen, C.; Li, Z.; Lin, H.; Wang, G.; Liao, J.; Li, M.; Lv, S.; Li, W. Enhanced Visible Light Photocatalytic Performance of ZnO Nanowires Integrated with CdS and Ag_2S. *Dalton Trans.* **2016**, *45*, 3750–3758. DOI: 10.1039/C5DT04533A.

[16] Luo, Y.; Jia, Y.; Zhang, D.; Cheng, X. Coaxial Electrospinning Method for the Preparation of TiO2 @CdS/PVA Composite Nanofiber Mat and Investigation on its Photodegradation Catalysis. *Photochem. Photobiol.* **2016**, *92*, 515–522. DOI: 10.1111/php.12591.

[17] Karimipour, M.; Molaei, M. Red Florescent Ag_2S-CdS Hybrid Nanoparticles Prepared by a One Pot and Rapid Microwave Method. *Electron. Mater. Lett.* **2016**, *12*, 205–210. DOI: 10.1007/s13391-015-5278-4.

[18] Vattikuti, S. V. P.; Byon, C.; Reddy, C. V. ZrO_2/MoS_2 Heterojunction Photocatalysts for Efficient Photocatalytic Degradation of Methyl Orange. *Electron. Mater. Lett.* **2016**, *12*, 812–823. DOI: 10.1007/s13391-016-6267-y.

[19] An, L.; Wang, G.; Cheng, Y.; Zhao, L.; Gao, F.; Cheng, Y. Synthesis of CdS/ZnO Nanocomposite and Its Enhanced Photocatalytic Activity in Degradation of Methyl Orange Russ. *Russ. J. Phys. Chem.* **2015**, *89*, 1878–1883. DOI: 10.1134/S0036024415100180.

[20] Dehmukh, K.; Mukherjee, M.; Bhushan, S. Structural and Optical Studies on La Doped CdS Nanocrystalline Films. *Turk. J. Phys.* **2012**, *361*, 9–21. DOI: 10.3906/fiz-1102-1.

[21] Vaizoğullar, A. İ. Needle-Like La-Doped MgO Photocatalyst: Synthesis, Characterization and Photodegradation of Flumequine Antibiotic under UV Irradiation. *J. Elec. Mater.* **2018**, *47*, 6751–6758. DOI: 10.1007/s11664-018-6591-0.

[22] Zhou, Q.; Li, L.; Xin, Z.; Yu, Y.; Wang, L.; Zhang, W. Visible Light Response and Heterostructure of Composite CdS@ZnS–ZnO to Enhance Its Photocatalytic Activity. *J. Alloys Compd.* **2020**, *813*, 152190. DOI: 10.1016/j.jallcom.2019.152190.

[23] Nie, R.; Shi, J.; Du, W.; Hou, Z. Ni_2O_3-around-Pd Hybrid on Graphene Oxide: An Efficient Catalyst for Ligand-Free Suzuki–Miyaura Coupling Reaction. *Appl. Catal. A-Gen.* **2014**, *473*, 1–6. DOI: 10.1016/j.apcata.2013.12.029.

[24] Ahmed, B.; Kumar, S.; Kumar, S.; Ojha, A. K. Shape Induced Spherical, Sheets and Rods, Optical and Magnetic Properties of CdS Nanostructures with Enhanced Photocatalytic Activity for Photodegradation of Methylene Blue Dye under Ultra-Violet Irradiation. *J. Alloys Compd.* **2016**, *679*, 324–334. DOI: 10.1016/j.jallcom.2016.03.295.

[25] Cui, H.; Zhou, Y.; Mei, J.; Li, Z.; Xu, S.; Yao, C. Synthesis of CdS/BiOBr Nanosheets Composites with Efficient Visible-Light Photocatalytic Activity. *Phys. Chem. Solids* **2018**, *112*, 80–87. DOI: 10.1016/j.jpcs.2017.09.011.

[26] Kganyago, P.; Mahlaule-Glory, L. M.; Mathipa, M. M.; Ntsendwana, B.; Mketo, N.; Mbita, Z.; Hintsho-Mbita, N. C. Synthesis of NiO Nanoparticles via a Green Route Using Monsonia Burkeana: The Physical and Biological Properties. *J. Photochem. Photobiol. B Biol.* **2018**, *182*, 18–26. DOI: 10.1016/j.jphotobiol.2018.03.016.

[27] Fan, H. M.; Fan, X. F.; Ni, Z. H.; Shen, Z. X.; Feng, Y. P.; Zou, B. S. Orientation-Dependent Raman Spectroscopy of Single Wurtzite CdS Nanowires. *J. Phys. Chem. C* **2008**, *112*, 1865–1870. DOI: 10.1021/jp7096839.

[28] Shen, S.; Guo, L. Growth of Quantum-Confined CdS Nanoparticles inside Ti-MCM-41 as a Visible Light Photocatalyst. *Mater. Res. Bull.* **2008**, *43*, 437–446. DOI: 10.1016/j.materresbull.2007.02.034.

[29] Reddy, D. A.; Choi, J.; Lee, S.; Kim, Y.; Hong, S.; Kumar, D. P.; Kim, T. K. Hierarchical Dandelion-Flower-like Cobalt-Phosphide Modified CdS/Reduced Graphene oxide-MoS_2 Nanocomposites as a Noble-Metal-Free Catalyst for Efficient Hydrogen Evolution from Water. *Catal. Sci. Technol.* **2016**, *6*, 6197–6206. DOI: 10.1039/C6CY00768F.

[30] Reddy, N. L.; Rao, V. N.; Kumari, M. M.; Ravi, P.; Sathish, M.; Shankar, M. V. Effective Shuttling of Photoexcitons on CdS/NiO Core/Shell Photocatalysts for Enhanced Photocatalytic Hydrogen Production. *Mater. Res. Bull.* **2018**, *101*, 223–231. DOI: 10.1016/j.materresbull.2018.01.043.

[31] Gonzalez-Elipe, A. R.; Holgado, J. P.; Alvarez, R.; Munuera, G. Use of Factor Analysis and XPS to Study Defective Nickel Oxide. *J. Phys. Chem.* **1992**, *96*, 3080–3086. DOI: 10.1021/j100186a056.

[32] Channei, D.; Chansaenpak, K.; Jannoey, P.; Phanichphant, S. The Staggered Heterojunction of CeO_2/CdS Nanocomposite for Enhanced Photocatalytic Activity. *Solid State Sci.* **2019**, *96*, 105951. DOI: 10.1016/j.solidstatesciences.2019.105951.

[33] Li, J.; Qian, X.; Peng, Y.; Lin, J. Hierarchical Structure NiO/CdS for Highly Performance H_2 Evolution. *Mater. Lett.* **2018**, *224*, 82–85. DOI: 10.1016/j.matlet.2018.04.083.

[34] Jouini, K.; Raouafi, A.; Dridi, W.; Daoudi, M.; Mustapha, B.; Chtourou, R.; Hosni, F. Investigation of Gamma-Ray Irradiation Induced Phase Change from NiO to Ni_2O_3 for Enhancing Photocatalytic Performance. *Optik* **2019**, *195*, 163109. DOI: 10.1016/j.ijleo.2019.163109.

[35] Mochizuki, S.; Saito, T. Intrinsic and Defect-Related Luminescence of NiO. *Physica B Condens. Matter* **2009**, *404*, 4850–4853. DOI: 10.1016/j.physb.2009.08.166.

[36] Vázquez, A.; Hernández-Uresti, D. B.; Obregón, S. Electrophoretic Deposition of CdS Coatings and Their Photocatalytic Activities in the Degradation of Tetracycline Antibiotic. *Appl. Surf. Sci.* **2016**, *386*, 412–417. DOI: 10.1016/j.apsusc.2016.06.034.

[37] Cai, W.; Li, Z.; Sui, J. A Facile Single-Source Route to CdS Nanorods. *Nanotechnology* **2008**, *19*, 465606. DOI: 10.1088/0957-4484/19/46/465606.

[38] Deng, C.; Hu, H.; Yu, H.; Wang, M.; Ci, M.; Wang, L.; Zhu, S.; Wu, Y.; Le, H. 1D Hierarchical CdS NPs/NiO NFs Heterostructures with Enhanced Photocatalytic Activity under Visible Light Irradiation. Adv. Powder *Technol.* **2020**, 465606–465212. DOI: 10.1016/j.apt.2020.06.003.

[39] Yang, T.; Peng, J.; Zheng, Y.; He, X.; Hou, Y.; Wu, L.; Fu, X. Enhanced Photocatalytic Ozonation Degradation of Organic Pollutants by ZnO Modified TiO2 Nanocomposites. Appl. Catal. *B* **2018**, *221*, 223–234. DOI: 10.1016/j.apcatb.2017.09.025.

[40] Kannusamy, P.; Sivalingam, T. Chitosan–ZnO/Polyaniline Hybrid Composites: Polymerization of Aniline with Chitosan–ZnO for Better Thermal and Electrical Property. *Polym. Degrad. Stabil.* **2013**, *98*, 988–996. DOI: 10.1016/j.polymdegradstab.2013.02.015.

[41] Alipour, A.; Lakouarj, M. M. Photocatalytic Degradation of RB Dye by CdS-Decorated Nanocomposites Based on Polyaniline and Hydrolyzed Pectin: Isotherm and Kinetic. *J. Environ. Chem. Eng.* **2019**, *7*, 102837. DOI: 10.1016/j.jece.2018.102837.

[42] Yi, H.; Jiang, M.; Huang, D.; Zeng, G.; Lai, C.; Qin, L.; Zhou, C.; Li, B.; Liu, X.; Cheng, M.; et al. Advanced Photocatalytic Fenton-like Process over Biomimetic hemin-Bi_2WO_6 with Enhanced pH. *J. Taiwan Inst. Chem. E* **2018**, *93*, 184–192. DOI: 10.1016/j.jtice.2018.06.037.